JOURNAL OF AIRCRAFT
Vol. 36, No. 2, March–April 1999

Flow Computations Around Delta Wings Using Unstructured Hybrid Grids

Shintaro Kano* and Kazuhiro Nakahashi†
Tohoku University, Sendai 980-8579-01, Japan

The capability of an unstructured hybrid grid method to compute the compressible Navier–Stokes equations is discussed for vortical flows over slender delta wings at low subsonic, high-alpha conditions as a basic study of off-design aerodynamics of high speed civil transport configurations. Computations of these flows require high resolutions of the boundary layers on the wing and of the vortical flow region above the wing. The unstructured hybrid grid, which is composed of a prismatic grid in boundary layers and tetrahedral and pyramidal grids for the remaining region, is used to treat such viscous flows. The compressible Navier–Stokes equations are solved on the hybrid grid by a cell-vertex, upwind finite volume method. The lower–upper–symmetric Gauss–Seidel implicit time integration scheme is used for the convergence acceleration to steady state. The numerical accuracy of the present method is discussed by comparing with the experimental data for the same configurations. It is demonstrated that the present hybrid grid method is efficient and accurate enough to predict the vortical flow fields over the delta wings.

Introduction

INVESTIGATIONS of the next generation supersonic transport, such as the high speed civil transport (HSCT), have been internationally conducted with a stronger and more focused interest in recent years. However, for developing a HSCT that is economically viable and environmentally acceptable, there are various technical problems to be solved. From an economical point of view, the improvement of lift-to-drag ratio (L/D) in supersonic cruise condition is one of the most important issues. A low-aspect-ratio, highly swept cranked delta and arrow wing planform is the common choice to maximize the cruise L/D. However, the arrow planform also has a pitch-up problem at high angles of attack during transonic and low-speed flight conditions. This is caused by a complex flow feature caused by leading-edge vortex, flow separation, and vortex breakdown.[1]

For the HSCT to be environmentally acceptable, the off-design condition at takeoff and landing is another important issue to be investigated. Airport noise regulation requires the HSCT to maintain low noise at takeoff and landing, and reasonable field length performance. To clear this environmental hurdle, one needs an aerodynamically sophisticated design of relatively high L/D at the high-alpha condition. This crucial requirement, along with the need for high L/D at supersonic flight conditions, necessitates variable leading and trailing edges to continuously optimize the drag caused by lift for each of the flight conditions. For such a design, understanding and controlling the development of leading-edge vortex separation, responsible for the nonlinear lift, is the key factor to maximizing the off-design performance and to providing desirable stability characteristics.[2]

In this paper, a numerical method developed to analyze the flow around a complete HSCT configuration is discussed in detail. One of the most difficult problems to compute such a flow around complex geometries is to generate a computational grid. Tetrahedral unstructured grid methods may be appropriate to treat such a complex configuration. However, their applications are mainly limited to inviscid flows because of the lack of accuracy to resolve the boundary layer on the wings. The CPU time and memory overheads are also major issues that need to be addressed. To address these issues, a hybrid grid method has been developed.[3,4] The grid is composed of a prismatic semistructured grid in the boundary layer and a tetrahedral fully unstructured grid in the remaining region. The prismatic layer is necessary to resolve the thin boundary layer developed along the surface accurately. The tetrahedral grid resolves the grid generation issue for the complex configuration.

Although several hybrid methods appear in the literature,[4,5] their verification of accuracy and capability to treat real engineering problems seems to be relatively unexplored. The objective of this paper is to discuss the capability of the hybrid grid method to compute the three-dimensional Navier–Stokes equations about a slender delta wing and a double-delta wing at low-speed and high-angle-of-attack conditions as a basic study of off-design aerodynamics of HSCT configurations. These delta wing configurations have been investigated experimentally and numerically by many researchers. Most of the computational results were obtained using structured grids. Also, these configurations are so sensitive to the local grid resolution that they are good test cases for assessing the numerical accuracy of the present hybrid grid approach.

Hybrid Grid

Developments of unstructured grid methods have been accelerated from the mid-1980s because of their attractive capabilities for complex configurations. Their usefulness has already been demonstrated for full aircraft calculations. These successes are a result of the developments of numerical algorithms for unstructured grids, efficient generation algorithms for tetrahedral grids using the advancing front method and the Delaney triangulation, and grid refinement procedures. Good reviews about the unstructured grid method are given in Refs. 6 and 7.

Despite these improvements, unstructured grid methods could not attain superiority over structured grid methods until recently, particularly for high Reynolds number viscous flows. This was mainly because of the painful inefficiency and mem-

Presented as Paper 98-0232 at the AIAA 36th Aerospace Sciences Meeting, Reno, NV, Jan. 12–15, 1998; received April 8, 1998; revision received Sept. 11, 1998; accepted for publication Sept. 14, 1998.

*Graduate Student, Department of Aeronautics and Space Engineering.

†Professor, Department of Aeronautics and Space Engineering. Associate Fellow AIAA.

ory overhead for the unstructured grid methods as compared with the available structured grid methods. Because of the unstructured distributions of grid points, simple explicit schemes had been generally employed for integrating the Euler and Navier–Stokes equations to a steady state. In addition, many three-dimensional unstructured schemes require the excessive memory overheads, which severely limit the size of the meshes, and hence, the class of problems to which they are applied. These problems become much worse for high Reynolds number viscous flow computations. More precisely, accurate resolution of the thin boundary layers developed along the wall surface requires very fine grid that causes a stiffness problem of the flow solver. Moreover, the generation of such a fine and stretched grid near wall is another challenging issue of the unstructured grid methods. Several important advancements were made in the tetrahedral grid method to overcome these problems for solving viscous flows.[8–10]

In contrast to the fully tetrahedral grid method, we use a hybrid grid that is composed of a structured or a semistructured grid for the near-wall viscous region, and an unstructured grid for the remainder of the computational domain. As mentioned before, accurate resolution of the thin boundary layers requires a highly dense grid near wall. Therefore, a big percentage of the CPU time and the memory requirement is consumed in this region, even for structured grid approaches. If we use a tetrahedral grid in this region, the number of cells becomes at least five times more than that of a hexagonal structured grid with the same number of grid points, as discussed by Barth.[11] This increase in the number of cells directly reflects on the required computational time and memory without much improvement in accuracy. By using prismatic cells, the number of cells in the boundary-layer region becomes approximately one-third of the tetrahedral grid. It is also apparent that a laminated grid rather than the tetrahedral grid is more suitable in the boundary-layer region for accurately computing the viscous terms.[12]

Grid Generation

The grid generation process is divided into two steps: surface grid generation and volume grid generation.

Triangular Surface Grid Generation

Surface grids of three-dimensional bodies are generated by the direct surface meshing method.[13] This method applies the advancing front approach directly to the body surface in the physical space. It does not rely on a mapping, so that the mesh size can be automatically controlled by adapting to the local surface curvature. Without mapping, surface definition for meshing can be more flexible.

Hybrid Volume Grid Generation

The hybrid grids comprised of tetrahedra, prisms, and pyramids are generated by the method described in Ref. 3. The prismatic semistructured grid is generated around viscous boundary surfaces, and is intended to cover the viscous regions of the flow. The tetrahedral grid covers the rest of the computational domain. The Delaunay incremental insertion method for tetrahedral grid generation is used. The prismatic grid is structured in directions normal to the boundary faces. To enhance the geometrical flexibility of the hybrid grid, the number of prismatic layers generated from one boundary face is variable from face to face. Therefore, if an inappropriate prism is produced, the advancement from the face is terminated. As a result, a stepped inflated boundary surface is formed. Unlike conventional prismatic grid generators, this technique works well even in regions having cavities and gaps. Pyramidal elements appear between tetrahedra and prisms. This method has shown its robustness for a variety of geometries without user intervention.[3,14] Only boundary surface triangulation must be specified.

Adaptive Grid Refinement

To increase resolution of the flowfield, adaptive grid refinement is implemented in the hybrid grid. In the region of tetrahedral unstructured grid, a tetrahedra bisection algorithm is used.[15,16] The prisms are refined directionally to preserve the structure of the mesh along the normal-to-surface direction in case hanging nodes are on the edges of the prisms.

We utilize the refinement criterion based on the values of second-order differences as

$$E_i = \max_e \left(\frac{|\nabla w_e - \overline{\nabla w_i}|}{|\nabla w_e| + |\nabla w_i| + \varepsilon |w_i| d^{-1}} \right) \tag{1}$$

where e denotes the elements surrounding node i, d is the diameter of the cell, and ε is the filter coefficients. Gas density is generally used for the monitor variable w.

Solution Algorithm

The fluid motion is governed by the time-dependent Navier–Stokes equations for an ideal gas. The equations are given in the nondimensional integral form as follows:

$$\frac{\partial}{\partial t} \int_\Omega \boldsymbol{Q}\, dV + \int_{\partial\Omega} [\boldsymbol{F}(\boldsymbol{Q}) - \boldsymbol{G}(\boldsymbol{Q})] \cdot \boldsymbol{n}\, dS = 0 \tag{2}$$

where $\boldsymbol{Q} = [\rho, \rho u, \rho v, \rho w, e]^T$ is the vector of conservative variables; ρ is the density; u, v, w are the velocity components in the x, y, z directions, respectively; and e is the total energy. The vectors $\boldsymbol{F}(\boldsymbol{Q})$ and $\boldsymbol{G}(\boldsymbol{Q})$ represent the inviscid and viscous flux vectors, respectively; and $\boldsymbol{n}$ is the outward normal to $\partial\Omega$, which is the boundary of the control volume Ω. This system of equations is completed by the perfect gas equation of state.

The equations are solved by a finite volume cell–vertex scheme. The control volume is a nonoverlapping dual cell whose boundary is shown in Fig. 1. The boundary surface is defined by the tetrahedra centroid C, face centroids B and D, and edge midpoint A. With this control volume, Eq. (2) can be written in an algebraic form as follows:

$$\frac{\partial \boldsymbol{Q}_i}{\partial t} = -\frac{1}{V_i} \sum_{j(i)} \Delta S_{ij} \boldsymbol{h}(\boldsymbol{Q}_{ij}^+, \boldsymbol{Q}_{ij}^-, \boldsymbol{n}_{ij}) + \frac{1}{V_i} \sum_{j(i)} \Delta S_{ij} \boldsymbol{G}(\boldsymbol{Q}_{ij}, \boldsymbol{n}_{ij}) \tag{3}$$

where ΔS_{ij} is a segment area of the control volume boundary associated with edge connecting points i and j. This segment area ΔS_{ij}, as well as its unit normal $\boldsymbol{n}_{ij}$, can be computed by summing up the contribution from each tetrahedron sharing the edge. The term $\boldsymbol{h}$ is an inviscid numerical flux vector normal to the control volume boundary, and $\boldsymbol{Q}_{ij}^{\pm}$ are values on both sides of the control volume boundary. The subscript of summation, $j(i)$, refers to all node points connected to node i.

If we evaluate $\boldsymbol{Q}_{ij}^{\pm}$ in $\boldsymbol{h}$ at both endpoints of each edge, we get the first-order scheme. Here we use the Harten-Lax-van Leer-Einfeldt-Wada (HLLEW) Riemann solver.[17] Second-order spatial accuracy is realized by linear reconstruction of the primitive variables $\boldsymbol{q} = [\rho, u, v, w, p]^T$, inside the control volume, viz.,

$$\boldsymbol{q}(x, y, z) = \boldsymbol{q}_i + \psi_i \nabla \boldsymbol{q}_i \cdot (\boldsymbol{r} - \boldsymbol{r}_i) \tag{4}$$

where $\boldsymbol{r}$ is a position vector pointing to (x, y, z); and i is the node number. The gradients associated with the control-volume centroids are volume-averaged gradients computed using the value in the surrounding grid cells. ψ $(0 \le \psi \le 1)$ is a limiter to make the scheme monotone. Here, Venkatakrishnan's limiter[18] is used because of its superior convergence properties.

To compute the viscous stresses and the heat flux terms in $\boldsymbol{G}(\boldsymbol{Q})$, spatial derivatives of the primitive variables at each control volume face are evaluated directly at the edges. In this paper, unless stated, all flow problems were treated as laminar flows. A one-equation turbulence model by Goldberg and Ra-

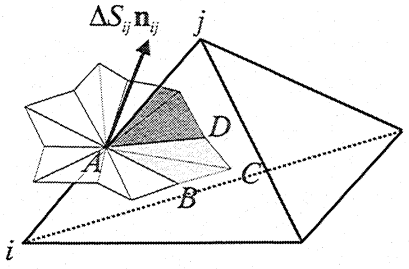

Fig. 1 Control volume.

makrishnan (G–R)[19] was implemented to treat turbulent flows. This turbulence model does not require a searching procedure along normal lines to the wall as required by the Baldwin–Lomax algebraic model. Therefore, it is suitable for the present unstructured grid method for treating complex geometries.

An implicit time-integration method is required for computing the high Reynolds number flows because of the severe Courant–Friedrichs–Lewy (CFL) condition as a result of having a very fine grid near the wall. Here the lower–upper–symmetric Gauss–Seidel (LU–SGS) implicit method[4,20,21] is applied to integrate Eq. (3) in time. With $\Delta \boldsymbol{Q} = \boldsymbol{Q}^{n+1} - \boldsymbol{Q}^n$, an implicit time integration of Eq. (3) can be written as

$$\Delta \boldsymbol{Q}_i = -\frac{\Delta t}{V_i} \sum_{j(i)} \Delta S_{ij} \boldsymbol{h}_{ij}^{n+1} + \frac{\Delta t}{V_i} \sum_{j(i)} \Delta S_{ij} \boldsymbol{G}_{ij}^{n} \tag{5}$$

By linearizing and splitting the numerical flux vector as $\boldsymbol{h}_{ij}^{n+1} = \boldsymbol{h}_{ij}^{n} + \boldsymbol{A}_i^{+} \Delta \boldsymbol{Q}_i + \boldsymbol{A}_j^{-} \Delta \boldsymbol{Q}_j$, and following a similar procedure to that used for the conventional derivation of the LU–SGS on a structured grid,[22] we obtain the following equations:

$$\left(\frac{V_i}{\Delta t} \boldsymbol{I} + \sum_{j(i)} \Delta S_{ij} \boldsymbol{A}_i^{+} \right) \Delta \boldsymbol{Q}_i + \sum_{j(i)} \Delta S_{ij} \boldsymbol{A}_j^{-} \Delta \boldsymbol{Q}_j = \boldsymbol{R}_i \tag{6}$$

where

$$\boldsymbol{R}_i = -\sum_{j(i)} \Delta S_{ij} \boldsymbol{h}_{ij}^{n} + \sum_{j(i)} \Delta S_{ij} \boldsymbol{G}_{ij}^{n} \tag{7}$$

The LU–SGS method on a unstructured grid can be derived by splitting node points $j(i)$ into two groups, $j \in L(i)$ and $j \in U(i)$ for the second summation in the left-hand side of Eq. (6):

$$\left[\frac{V_i}{\Delta t} \boldsymbol{I} + \sum_{j(i)} \Delta S_{ij} \boldsymbol{A}_i^{+} \right] \Delta \boldsymbol{Q}_i + \sum_{j \in L(i)} \Delta S_{ij} \boldsymbol{A}_j^{-} \Delta \boldsymbol{Q}_j + \sum_{j \in U(i)} \Delta S_{ij} \boldsymbol{A}_j^{-} \Delta \boldsymbol{Q}_j = \boldsymbol{R}_i \tag{8}$$

This can be solved using the following two sweeps:

Forward sweep:

$$\Delta \boldsymbol{Q}_i^{*} = \boldsymbol{D}^{-1} \left[\boldsymbol{R}_i - \sum_{j \in L(i)} \Delta S_{ij} \boldsymbol{A}_j^{-} \Delta \boldsymbol{Q}_j^{*} \right] \tag{9a}$$

Backward sweep:

$$\Delta \boldsymbol{Q}_i = \Delta \boldsymbol{Q}_i^{*} - \boldsymbol{D}^{-1} \sum_{j \in U(i)} \Delta S_{ij} \boldsymbol{A}_j^{-} \Delta \boldsymbol{Q}_j \tag{9b}$$

where

$$\boldsymbol{D} = \left(\frac{V_i}{\Delta t} \boldsymbol{I} + \sum_{j(i)} \Delta S_{ij} \boldsymbol{A}_i^{+} \right) \tag{10}$$

The term $\boldsymbol{D}$ is diagonalized by using the Jameson and Turkel approximation of the Jacobian[23] as $\boldsymbol{A}^{\pm} = 0.5(\boldsymbol{A} \pm \rho_A \boldsymbol{I})$, where ρ_A is a spectral radius of the Jacobian $\boldsymbol{A}$. For viscous flows, ρ_A is replaced by

$$\rho_A^{*} = \rho_A + 2 \frac{\mu + \mu_T}{Re \cdot \rho \cdot h} \tag{11}$$

where μ and μ_T are kinetic and turbulent viscosities, respectively; and h is the distance between i and j.

Using the fact that $\Sigma_{j(i)} \Delta S_{ij} \boldsymbol{A} = 0$,[21] Eq. (10) becomes a diagonal matrix:

$$\boldsymbol{D} = \left[\frac{V_j}{\Delta t} + 0.5 \sum_{j(i)} \Delta S_{ij} \rho_A \right] \boldsymbol{I} \tag{12}$$

With these simplifications, the final form of the LU–SGS method for the unstructured grid becomes the following sweeps:

Forward sweep:

$$\Delta \boldsymbol{Q}_i^{*} = \boldsymbol{D}^{-1} \left[\boldsymbol{R}_i - 0.5 \sum_{j \in L(i)} \Delta S_{ij} (\Delta \boldsymbol{h}_j^{*} - \rho_A \Delta \boldsymbol{Q}_j^{*}) \right] \tag{13a}$$

Backward sweep:

$$\Delta \boldsymbol{Q}_i = \Delta \boldsymbol{Q}_i^{*} - 0.5 \boldsymbol{D}^{-1} \sum_{j \in U(i)} \Delta S_{ij} (\Delta \boldsymbol{h}_j - \rho_A \Delta \boldsymbol{Q}_j) \tag{13b}$$

where $\Delta \boldsymbol{h} = \boldsymbol{h}(\boldsymbol{Q} + \Delta \boldsymbol{Q}) - \boldsymbol{h}(\boldsymbol{Q})$

The lower/upper splitting of Eq. (8) for the structured grid is realized by using the hyperplanes $i + j + k = \text{const}$. For the unstructured grid, there are no grid lines, and so a different strategy is necessary to perform the sweeps. In Ref. 21, it was proposed that sweep be conducted, starting from node 1 to N and backward. Namely, lower nodes $j \in L(i)$ are surrounding nodes whose number is less than i. The upper nodes $j \in U(i)$ are surrounding nodes whose number exceeds the current node number i. Here, we employ a grid reordering technique[4] to improve the convergence and the vectorization. Details of this grid reordering technique are described in Ref. 4.

This solution method is applicable to arbitrary unstructured grids. No matrix inversion is required, and the CPU cost of one LU–SGS iteration is ~70% of one vectorized explicit time step. The present code requires 65×10^{-6} s per node per step on 1 CPU of Cray C90. The code is experimentally found to be stable for CFL numbers up to 1×10^{6}. The number of iterations required for the convergence is usually about less than 3000 steps. The present code requires about 180 words per node. Extra memory required for the implicit method is approximately 5% of the total memory requirement.

Accuracy of the flow solver for viscous flows was examined by several basic flow problems. At first, a laminar boundary-layer flow on a flat plate was computed by the present approach. The predicted velocity profile showed a good agreement with the Blasius solution. We also computed a turbulent boundary layer on a flat plate with the G–R one-equation turbulence model.[19] It showed good accordance with the theory. The code was also applied to a transonic flow around the Onera-M5 airplane, and a hypersonic flow around a double ellipsoid for the validation.[4]

Results

Seventy-Six Degree Delta Wing

Numerical accuracy of the present method was investigated for a flow over a slender delta wing of aspect ratio 1, corresponding to a sweep angle of 76 deg, at a high angle of attack. This flowfield has been studied both experimentally[24,25] and computationally,[26,27] and the overall physical structure of the flow is well understood. The characteristics of the flowfield are dominated by two counter-rotating primary vortices that form

over the wing because of separation at the leading edge. These vortices induce suction pressures over the upper surface of the wing and cause a nonlinear increase in lift over that attainable through attached flow. The adverse pressure gradients induced by the primary vortex can also lead to secondary vortices. The maximum lift attained with increasing angle of attack is associated with the onset of vortex breakdown at the trailing edge. With further increases in angle of attack, the vortex breakdown point moves farther forward on the wing until, at a sufficiently high angle of attack, the flow is dominated by the periodic wake shedding encountered over bluff bodies.

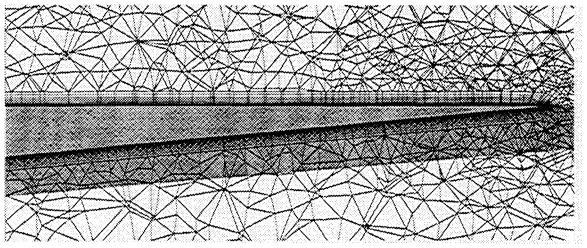

Fig. 2 Cut view of the hybrid grid at $x = 0.5$ for a 76-deg delta wing.

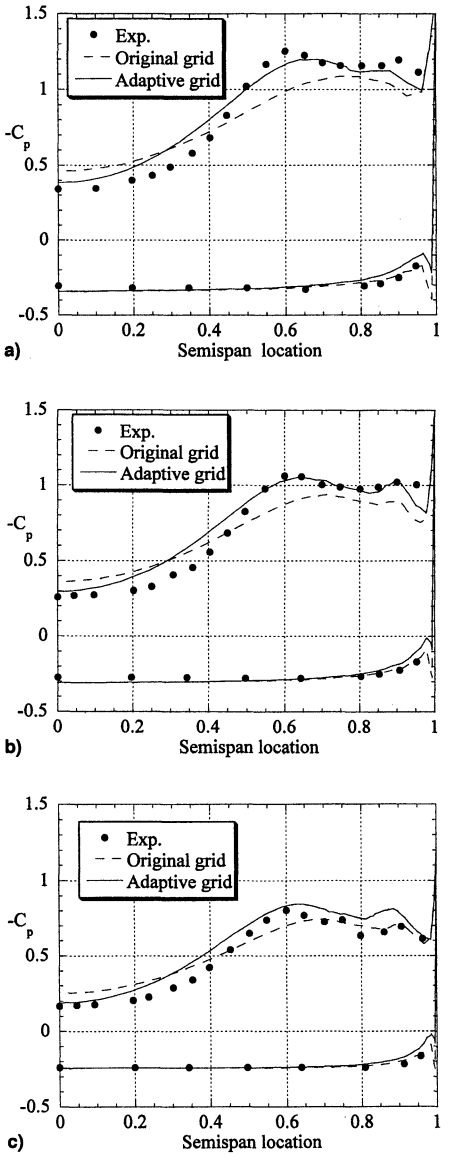

Fig. 3 Surface pressure distribution at x = a) 0.3, b) 0.5, and c) 0.7 for $M_\infty = 0.3$, $Re_c = 0.95 \times 10^6$, and $\alpha = 20.5$ deg.

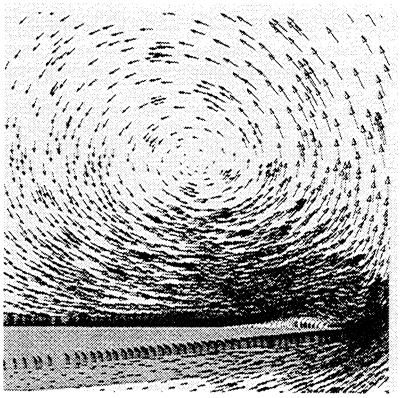

Fig. 4 Velocity vector on a cut view at $x = 0.7$ for $M_\infty = 0.3$, $Re_c = 0.95 \times 10^6$, and $\alpha = 20.5$ deg.

The axial direction coincides with the wing chord direction, and the wing apex is at $x = 0$ and the trailing edge is at $x = 1$. Flow conditions were freestream Mach number, $M_\infty = 0.3$, Reynolds number based on root chord, $Re_c = 0.95 \times 10^6$, and an angle of attack of 20.5 deg. The computational results were compared with the available experimental measurements of Hummel[24] and Kjelgaard and Sellers.[25] The geometry used here was identical to the geometry used by Hummel, and similar to that of Kjelgaard and Seller. In Hummel's experiment, the Reynolds number was $Re_c = 0.95 \times 10^6 (M_\infty \approx 0.1)$, and in Kjelgaard and Seller's experiment, $Re_c = 1.0 \times 10^6 (M_\infty \approx 0.3)$. Here, the Reynolds number was taken from Hummel's experiment. However, the freestream Mach number was taken from the Kjelgaard and Seller's experiment because the compressibility effects were small as reported in Ref. 26. These experimental data have also been used to validate a number of numerical results at high angle of attack using structured grids.[26,27]

A close-up view of the hybrid grid in a transverse plane ($x = 0.5$) is shown in Fig. 2. As seen, prisms were generated to cover the boundary-layer regions of the wing, and the rest were composed of tetrahedra and pyramids. The outer boundary was a semisphere, whose radius was 10 root chord lengths. The first point above the surface was located at a distance of 10^{-4} root chord length. The total number of grid points for the initial grid is 302,810. The numbers of prismatic, pyramidal, and tetrahedral cells are 409,645, 63, and 510,289, respectively. Grid refinement was applied twice to the tetrahedral cells in the initial grid. The final number of grid point became 536,910.

Comparisons of the predicted surface pressure coefficients with the experimental data of Ref. 24 are shown in Figs. 3a–3c at longitudinal stations of $x = 0.3$, 0.5, and 0.7 respectively. At these stations, the overall levels of the predicted pressure coefficients obtained by the adaptive grid agrees well with the experimental results. In Fig. 4, a velocity vector plot in a transverse plane at $x = 0.7$ is shown. The primary and secondary vortices are clearly seen.

Double-Delta Wing

The flow over a double-delta wing is more complicated than that for the delta wing shown in Fig. 4. Here, separation vortices emanate from both the strake leading edge and the wing leading edge. At moderate angles of attack, these two vortices interact with each other in the main wing region. By comparison, the inboard vortex, originating from the strake leading edge, is relatively weak in the wing region. It is thus readily moved outboard by the induced velocity of the wing vortex, and the two vortices merge.

The body geometry is shown in Fig. 5. The leading-edge sweep angle is 80 deg at the strake and 60 deg at the wing. The thickness is 0.6% of the root chord, and the leading edge is rounded. A cut view of the hybrid grid at $x = 0.625$ for this wing is shown in Fig. 6. The prismatic layers are well gener-

ated over the surface. The minimum spacing at the surface is 8.0×10^{-5} of the root chord length. The number of total grid points is 728,210. The total number of cells is 2,061,361 where the number of prismatic cells is 1,025,189, the number of pyramids is 15,980, and number of tetrahedras is 1,020,192. The outer boundaries were located 10 chord lengths away from the body surface.

The computation was conducted at a freestream Mach number of 0.3, a Reynolds number $Re_c = 1.2 \times 10^6$, and an angle of attack of 12 deg. In Fig. 7, a perspective view of the computed total pressure contours at several chordwise stations is shown, where the main flow feature is clearly captured. However, the predicted spanwise pressure distributions at $x = 0.75$, shown in Fig. 8, are not well predicted. In this figure, the experimental data[28] are shown for the upper surface. The computed result is shown by solid lines for upper and lower surfaces. The predictions indicated that the computed strake vortex is weaker than that of the experiment. These results are similar to those of Refs. 29 and 30. Additional grid refinement

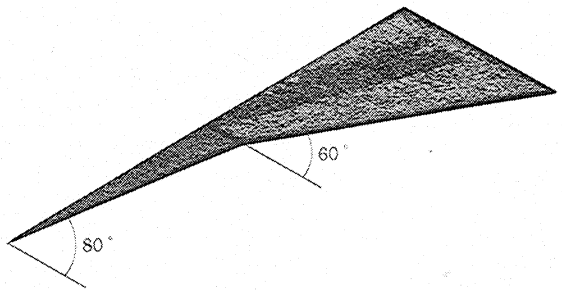

Fig. 5 Body geometry for a double-delta wing.

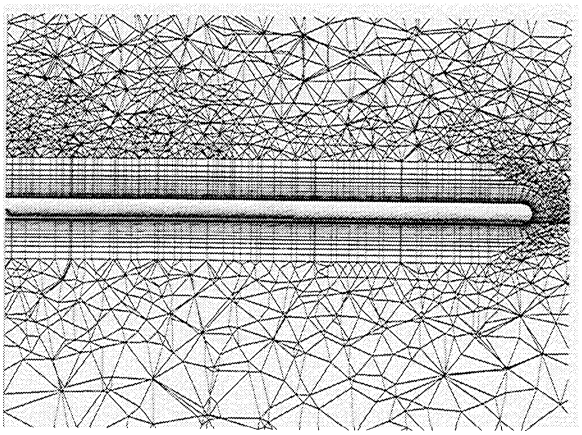

Fig. 6 Cut view of the hybrid grid at $x = 0.625$ for a double-delta wing.

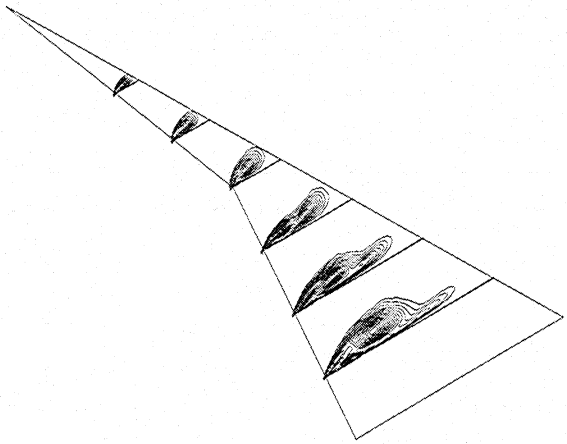

Fig. 7 Perspective view of the spanwise total-pressure contours plot for $M_\infty = 0.3$, $Re_c = 1.2 \times 10^6$, and $\alpha = 12$ deg.

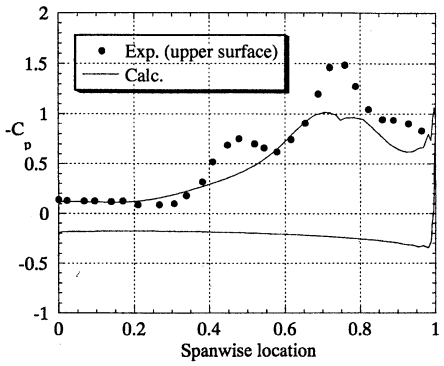

Fig. 8 Surface pressure distribution at $x = 0.75$ for $M_\infty = 0.3$, $Re_c = 1.2 \times 10^6$, and $\alpha = 12$ deg.

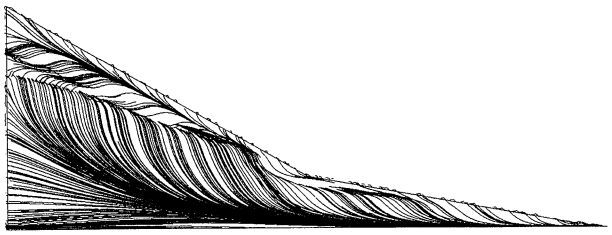

Fig. 9 Computed near-surface flow pattern for $M_\infty = 0.3$, $Re_c = 1.2 \times 10^6$, and $\alpha = 12$ deg.

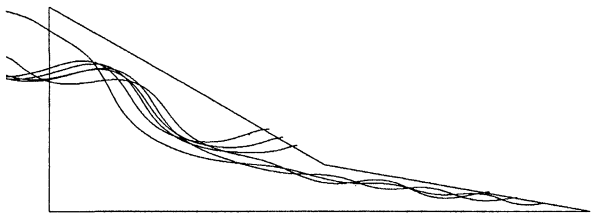

Fig. 10 Computed off-surface particle traces for $M_\infty = 0.3$, $Re_c = 1.2 \times 10^6$, and $\alpha = 12$ deg.

studies may be required to capture the strake vortex accurately. The surface streamlines and the streamlines over the wing are shown in Figs. 9 and 10, respectively. These results are qualitatively very similar to those obtained using the structured grid method of Ref. 30.

Conclusions

In this paper, the capability of the hybrid unstructured grid method was discussed for computations of vortical flowfields over delta wings as a basic study of off-design aerodynamics of HSCT configurations. The unstructured hybrid grid, composed of a prismatic grid in boundary layers and a tetrahedral grid for the remaining region, was used to treat such viscous flows. The use of prismatic cells in the boundary-layer region reduces the number of required cells in that region by about one-third compared with the fully tetrahedral grid. The compressible Navier–Stokes equations were solved on the hybrid grid by a cell–vertex, upwind finite volume method with the LU–SGS implicit time integration scheme. With a prismatic layer and an adaptive grid refinement, the boundary layer and the wing leading-edge vortex are well resolved. Because of the present method's suitability for treating complex configurations, it is deemed promising for the aerodynamic analysis and design of configurations such as the HSCT.

References

[1]Benoliel, A. M., and Mason, W. H., "Pitch-Up Characteristics for HSCT Class Planforms: Survey and Estimation," AIAA Paper 94-1819, June 1994.

[2]Nelson, C. P., "Effects of Wing Planform on HSCT Off-Design Aerodynamics," AIAA Paper 92-2629, June 1992.

[3]Sharov, D., and Nakahashi, K., "Hybrid Prismatic/Tetrahedral Grid Generation for Viscous Flow Applications," *AIAA Journal*, Vol. 36, No. 2, 1998, pp. 157–162.

[4]Sharov, D., and Nakahashi, K., "Reordering of Hybrid Unstructured Grids for Lower-Upper Symmetric Gauss-Seidel Computations," *AIAA Journal*, Vol. 36, No. 3, 1998, pp. 484–486.

[5]Parthasarathy, V., and Kallinderis, Y., "Adaptive Prismatic-Terahedral Grid Refinement and Redistribution for Viscous Flows," *AIAA Journal*, Vol. 34, No. 2, 1996, pp. 707–716.

[6]Deconinck, H., and Barth, T. (eds.), *Special Course on Unstructured Grid Methods for Advection Dominated Flows*, AGARD Rept. 787, May 1992.

[7]Venkatakrishnan, V., "A Perspective on Unstructured Grid Flow Solvers," AIAA Paper 95-0667, Jan. 1995.

[8]Frink, N. T., "Assessment of an Unstructured-Grid Method for Predicting 3-D Turbulent Viscous Flows," AIAA Paper 96-0292, Jan. 1996.

[9]Mavpilas, D. J., "Multigrid Strategies for Viscous Solvers on Anisotropic Unstructured Meshes," AIAA Paper 97-1952, June 1997.

[10]Pizadeh, S., "Viscous Unstructured Three-Dimensional Grids by the Advancing-Layer Method," AIAA Paper 94-0417, Jan. 1994.

[11]Barth, T. J., "Aspects of Unstructured Grids and Finite-Volume Solvers for the Euler and Navier-Stokes Equations," *Special Course on Unstructured Grid Methods for Advection Dominated Flows*, AGARD Rept. 787, 1992, pp. 1–61.

[12]Baker, T. J., "Discretization of the Navier Stokes Equations and Mesh Induced Errors," *5th International Conference on Numerical Grid Generation in Computational Field Simulations*, Mississippi State Univ., Mississippi State, MS, 1996, pp. 209–218.

[13]Nakahashi, K., and Sharov, D., "Direct Surface Triangulation Using the Advancing Front Method," AIAA Paper 95-1686, June 1995.

[14]Kodera, M., Nakahashi, K., Hiraiwa, T., Kanda, T., and Mitani, T., "Scramjet Inlet Flow Computations by Hybrid Grid Method," AIAA Paper 98-0962, Jan. 1998.

[15]Rivara, M. C., "Selective Refinement/Derefinement Algorithms for Sequences of Nested Triangulations," *International Journal of Numerical Methods in Engineering*, Vol. 28, No. 6, 1989, pp. 2889–2906.

[16]Sharov, D., and Fujii, K., "Three-Dimensional Adaptive Bisection of Unstructured Grids for Transient Compressible Flow Computations," AIAA Paper 95-1708, June 1995.

[17]Obayashi, S., and Guruswamy, G. P., "Convergence Acceleration of an Aeroelastic Navier-Stokes Solver," AIAA Paper 94-2268, Aug. 1994.

[18]Venkatakrishnan, V., "On the Accuracy of Limiters and Convergence to Steady State Solutions," AIAA Paper 93-0880, Jan. 1993.

[19]Goldberg, U. C., and Ramakrishnan, S. V., "A Pointwise Version of Baldwin-Barth Turbulence Model," *Computational Fluid Dynamics*, Vol. 1, 1993, pp. 321–338.

[20]Soetrisno, M., Imlay, S. T., and Roberts, D. W., "A Zonal Implicit Procedure for Hybrid Structured-Unstructured Grids," AIAA Paper 94-0645, Jan. 1994.

[21]Men'shov, I., and Nakamura, Y., "Implementation of the LU-SGS Method for an Arbitrary Finite Volume Discretization," *Proceedings of the Japanese 9th CFD Symposium*, Japan Society of Computational Fluid Dynamics, Tokyo, Japan, 1995, pp. 123, 124.

[22]Jameson, A., and Yoon, S., "Lower-Upper Implicit Schemes with Multiple Grids for the Euler Equations," *AIAA Journal*, Vol. 25, No. 7, 1987, pp. 929–935.

[23]Jameson, A., and Turkel, E., "Implicit Schemes and LU Decompositions," *Mathematics of Computation*, Vol. 37, No. 156, 1981, pp. 385–397.

[24]Hummel, D., "On the Vortex Formation over a Slender Wing at Large Angle of Incidence," *High Angle of Attack Aerodynamics*, AGARD, CP-247, 1979 (Paper 15).

[25]Kjelgaard, S. O., and Sellers, W. L., III, "Detailed Flowfield Measurements over a 75-Degree Swept Delta Wing for Code Validation," *Validation of Computational Fluid Dynamics*, Vol. 2, AGARD, CP-437, 1988 (Paper P10).

[26]Thomas, J. L., Krist, S. T., and Anderson, J. K., "Navier-Stokes Computations of Vortical Flows over Low-Aspect-Ratio Wings," *AIAA Journal*, Vol. 28, No. 2, 1990, pp. 205–212.

[27]Ekaterinaris, J. A., and Schiff, L. B., "Numerical Prediction of Vortical Flow over Slender Delta Wings," *Journal of Aircraft*, Vol. 30, No. 6, 1993, pp. 935–942.

[28]Hummel, D., "Documentation of Separated Flows for Computational Fluid Dynamics Validation," *AGARD Fluid Dynamics Panel Symposium on Validation of Computational Fluid Dynamics*, Vol. 2, AGARD, CP-437, 1988, pp. 1–24.

[29]Fujii, K., and Schiff, L. B., "Numerical Simulation of Vortical Flows over a Strake-Delta Wing," *AIAA Journal*, Vol. 27, No. 9, 1989, pp. 1153–1162.

[30]Hsu, C.-H., and Liu, C. H., "Navier-Stokes Computations of Flow Around a Round-Edged Double-Delta Wing," *AIAA Journal*, Vol. 28, No. 6, 1990, pp. 961–968.